

CLUMPY STREAMS FROM CLUMPY HALOS:
DETECTING MISSING SATELLITES WITH COLD STELLAR STRUCTURESJOO HEON YOON^{1*}, KATHRYN V. JOHNSTON¹, AND DAVID W. HOGG²*ApJ Submitted*

ABSTRACT

Dynamically cold stellar streams are ideal probes of the gravitational field of the Milky Way. This paper re-examines the question of how such streams might be used to test for the presence of “missing satellites” — the many thousands of dark-matter subhalos with masses $10^5 - 10^7 M_\odot$ which are seen to orbit within Galactic-scale dark-matter halos in simulations of structure formation in Λ CDM cosmologies. Analytical estimates of the frequency and energy scales of stream encounters indicate that these missing satellites should have a negligible effect on hot debris structures, such as the tails from the Sagittarius dwarf galaxy. However, long cold streams, such as the structure known as GD-1 or those from the globular cluster Palomar 5 (Pal 5) are expected to suffer many tens of direct impacts from missing satellites during their lifetimes. Numerical experiments confirm that these impacts create gaps in the debris’ orbital energy distribution, which will evolve into degree- and sub-degree-scale fluctuations in surface density over the age of the debris. Maps of Pal 5’s own stream contain surface density fluctuations on these scales. The presence and frequency of these inhomogeneities suggests the existence of a population of missing satellites in numbers predicted in the standard Λ CDM cosmologies.

Subject headings: cosmology: theory – dark matter – Galaxy: halo – Galaxy: kinematics and dynamics – Galaxy: structure

1. INTRODUCTION

Standard Λ CDM models of the Universe allow us to explain structure formation on large scales. However, they predict an order of magnitude more dark matter subhalos within the halos of typical galaxies than the number of known satellite galaxies orbiting the Milky Way (Klypin et al. 1999; Moore et al. 1999; Diemand et al. 2007; Springel et al. 2008). Recent, large-area stellar surveys have discovered dozens of new satellite galaxies, most notably using the Sloan Digital Sky Survey (SDSS, e.g. Willman et al. 2005; Belokurov et al. 2006a, 2007; Zucker et al. 2006; Irwin et al. 2007; Koposov et al. 2007; Walsh et al. 2007) but the number discrepancy between simulated dark matter subhalo and observed satellite populations is still significant. This discrepancy can partially be explained by accounting for the incomplete sky-coverage of SDSS and the distance-dependent limit on this survey’s sensitivity to low-surface brightness objects (Koposov et al. 2008; Tollerud et al. 2008). Indeed, models which take this into account and consider diffuse, (i.e. undetectable) satellite galaxies can reconcile the number counts for subhalos (Bullock et al. 2010). However, when they impose the suppression of stellar populations in low mass subhalos (which have masses below $5 \times 10^8 M_\odot$) the number of undetected galaxies significantly declines and the prediction of numerous purely dark matter subhalos less massive than $5 \times 10^8 M_\odot$ remains.

There could be a genuine absence of “missing satellites” in the inner halo due to destruction by disk

shocks, as illustrated in the calculations D’Onghia et al. (2010). However, note that these analytic descriptions of disk shocking based on the energy criterion are known to overestimate disruption rates of subhalos significantly (Goerdt et al. 2007). Once these destructive effects are accurately accounted for, proof of the existence (or lack) of these “missing satellites” could provide an important constraint on the nature of dark matter, which sets the minimum scale for the formation of dark matter subhalos (e.g. Hooper et al. 2007).

Along with the discovery of new satellite galaxies, SDSS has also uncovered a multitude of stellar structures in the Milky Way halo from disrupting globular clusters or satellite galaxies. In many cases, the debris is dynamically cold and distributed narrowly in space (Odenkirchen et al. 2001; Belokurov et al. 2006b; Lauchner et al. 2006; Grillmair & Johnson 2006; Grillmair & Dionatos 2006b; Grillmair 2006, 2009). Such cold stellar streams should be sensitive probes of the gravitational potential. On global scales, they can be used to constrain the radial profile, shape and orientation of the Milky Way’s triaxial dark matter halo (e.g. Johnston et al. 1999; Ibata et al. 2002; Johnston et al. 2005; Binney 2008; Eyre 2010; Koposov et al. 2010; Law & Majewski 2010). The presence of dark matter subhalos would add asymmetries to the global potential over a range of smaller scales which will perturb these cold streams or even destroy them. Hence, if the missing satellites do exist they will add random uncertainties to any stellar-dynamical assessment of the global potential.

Gravitational lensing has been suggested to be a useful tool to probe the presence of subhalos (Chiba 2002; Metcalf & Zhao 2002; Chen et al. 2003; Moustakas & Metcalf 2003; Metcalf et al. 2004; Keeton & Moustakas 2009; Riehm et al. 2009; Xu et al.

*jhyoon@astro.columbia.edu

¹Department of Astronomy, Columbia University, New York 10027, USA²Center for Cosmology and Particle Physics, Department of Physics, New York University, New York 10003, USA

2009). These investigations conclude that flux ratio anomalies in lensed images or lensing time delays could be caused by dark matter subhalos, though the constraints are limited by our knowledge of the spatial distribution of subhalos. However, this method is only applicable to the most massive and most centrally concentrated dark matter halos, and not to galaxies like the Milky Way more generally.

The effect of dark-matter subhalos on stellar streams has been explored in several previous studies. Ibata et al. (2002) showed that debris from the destruction of a $10^6 M_\odot$ globular cluster should be affected by heating due to repeated close encounters of subhalos and concluded that this effect could be detectable with future astrometric surveys. Moreover, Quinn et al. (2008) found that the inhomogeneities seen in Pal 5's tidal tails could not be accounted for in simulations evolved in a smooth potential. For the streams of larger satellites like the Sagittarius dwarf galaxy (hereafter Sgr), Johnston et al. (2002) found that although stars in the debris are scattered by encounters with dark matter subhalos, the thickness of the current Sgr stream could be explained as being due to the Large Magellanic Cloud alone. Siegal-Gaskins & Valluri (2008) tested the additional influence of different host potentials on debris from satellite galaxies and pointed out that while subhalos can shift the positions of streams and cause clumpy structures, the shape of the halo potential and orbital path can have an overall comparable effect. Most recently, Carlberg (2009) modeled a simplified stream on a circular orbit and concluded that dynamically old ($> 3\text{Gyr}$) stellar streams cannot survive in the presence of subhalos with the masses and numbers predicted by ΛCDM .

These previous works point to stellar streams as perhaps the most powerful way to find the missing satellites. However, none of these investigations separated the effect on streams of the known (and therefore uninteresting!) satellites with masses $> 10^8 M_\odot$ (Bovill & Ricotti 2009; Bullock 2010, and references therein) from those that are “missing” (the pure dark-matter subhalos). In this study we construct a framework for understanding stream inhomogeneities by first isolating and dissecting the characteristics of disturbances caused by dark-matter subhalos alone. In contrast to previous work, which looked at the overall response of cold streams to the complete ΛCDM subhalo mass spectrum, we look at the expected frequency, influence and characteristic observable signatures of subhalos in each mass decade separately. We also contrast the response of different streams to the same masses, from ribbons such as Pal 5 to the giant stream from Sgr. Our twin aims are: (i) to understand with which streams we are most likely to be able to conclusively prove the existence or absence of missing satellites; and (ii) to learn how signatures of missing satellites that are apparent in streams might be interpreted.

It should be noted that the discovery of very cold streams from globular clusters has inspired discussions of how the intrinsic properties of stellar streams themselves could cause inhomogeneities in their density distributions (Küpper et al. 2008, 2010; Quillen & Comparetta 2010) and these self-induced fluctuations could confuse the conclusive association of observed disturbances with dark-matter subhalo interactions. Our own work is

also motivated by these current observations which contain tantalizing suggestions of non-uniformity in some cold stellar streams (e.g. the structure known as GD-1 and those from the globular cluster Pal 5, see Odenkirchen et al. 2003; Grillmair & Dionatos 2006a,b; Koposov et al. 2010), as well as the prospect of the density of these streams being mapped more extensively (and accurately) in space and velocity with observations in the near future. Such observations could potentially distinguish between the effect of subhalo encounters on different mass scales as well differentiate these signatures from non-uniformities due to intrinsic stream dynamics.

We first review our understanding of the properties of dark-matter structures and stellar stream evolution in smooth potentials in §2. We use this understanding to make order-of-magnitude estimates for the frequency and effect of encounters of stellar streams with structures of different masses in §3. We then go on to illustrate these expectations with numerical experiments in §4 as well as discuss the observational signatures of these encounters in §5. We summarize our conclusions in §6.

2. BACKGROUND AND METHODS

The aim of this paper is to characterize the effects that dark matter subhalos orbiting around the Milky Way can have on debris from satellite disruption. In order to isolate the influence of subhalos from other factors, neither the debris distribution nor the Milky Way is modelled self-consistently, and a simplified form for the mass distribution is assumed in both cases. In particular, in our numerical experiments, the debris is represented by 3,000 test particles which orbit, along with a varying number of subhalos, in a smooth and spherical Milky Way halo. The orbits of the test particles and subhalos are integrated using the leap-frog method with a time-step of 0.5Myr. The test particles respond to the gravity of both the Milky Way halo and subhalos, but the subhalos do not interact with each other.

Note that our numerical approach misses several effects which could themselves contribute to non-uniform appearance of streams. These include multiple or continuous mass-loss, other asymmetries in the Galactic potential and self-gravity of the star streams. We will discuss each of these further in § 5.3.

The dark-matter distributions (both parent and subhalos) are chosen to mimic the end point of the Via Lactea II (VLII, Diemand et al. 2008) N-body simulation of structure formation on Galactic scales (see §2.1), while the distribution of tidal debris (and test particle orbits in our numerical experiments) are chosen to match expectations from N-body simulations of satellite destruction (see §2.2).

2.1. Dark Matter Halo Properties

The parent dark-matter distribution is a Milky-Way-like halo represented by a Navarro-Frenk-White (NFW) potential (Navarro et al. 1996):

$$\frac{\rho(r)}{\rho_{\text{crit}}} = \frac{\delta_c}{(r/r_s)(1 + r/r_s)^2} \quad (1)$$

with parameters chosen to match the VLII N-body simulation ($M_{\text{MW}} = 1.77 \times 10^{12} M_\odot$, $R_s = 24.6\text{kpc}$, $R_{\text{vir}} = 389\text{kpc}$, Diemand et al. 2008).

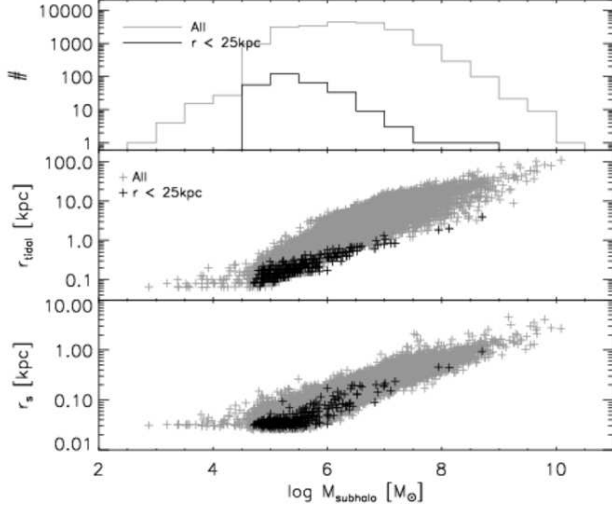


Figure 1. Number, scale radii (r_s) and tidal radii (r_{tidal}) of subhalos in VLII as a function of subhalo mass (M_{sub}). Gray points are for all subhalos and black are for those within 25 kpc at the present day.

We also assume the NFW form for the subhalos and directly take all physical properties (i.e. the masses, tidal and scale radii, see Figure 1) and orbits of subhalos from the publicly available analysis of the VLII simulation (Diemand et al. 2008). In practice, cosmological simulations like VLII have finite resolution, so the mass function is not complete below $4 \times 10^6 M_\odot$. We compensate for this resolution limit by duplicating subhalos within the mass range of $10^5 M_\odot - 10^7 M_\odot$ to maintain the power-law mass spectrum with a power law index -1 set by larger masses (see upper panel of Figure 1). As a result, each mass decade has 10 times more subhalos than the mass decade above. The orbits of the duplicated subhalos are set by rotating the position and velocity vectors of the original subhalos by random angles so as to preserve spherical symmetry and velocity isotropy of the subhalo population. This method retains the potential and kinetic energy of subhalos and their radial distribution.

2.2. Tidal Stream Properties

The general principle of debris evolution can be simply described: stars being torn from a satellite initially share a single orbital phase (or angle), but have a small range in orbital properties (or actions); this range in orbital properties corresponds to a range in orbital periods (or frequencies); and these period differences lead to gradual spreading of the debris along the satellite's original orbit (Johnston 1998; Helmi & White 1999). Note that this description of evolution as simply phase-mixing can break down for larger mass satellites (more than 0.01% of the mass of the parent) whose own gravity has been shown to influence the morphology of the debris (Choi et al. 2007). This effect is ignored in our work since we are mostly interested in lower mass satellites and in differences in debris distribution at smaller scales.

2.2.1. Scales in Debris

Johnston (1998) and Johnston et al. (2001) found that the distribution of debris particles observed in N-body

simulations of satellite disruption could be described in terms of the dimensionless *tidal scale*

$$s \equiv \left(\frac{m}{M_p} \right)^{1/3} \quad (2)$$

where m is the mass of a satellite and M_p is the mass of a host halo enclosed by the pericenter, R_p , of the satellite orbit. The *tidal radius* where the internal and tidal forces are in equilibrium and mass loss occurs scales as

$$r_{\text{tide}} \sim s R_p = \left(\frac{m}{M_p} \right)^{1/3} R_p. \quad (3)$$

The orbits of debris are offset in energy, E , and angular momentum J from the satellite's own orbital properties. The tidal scales can be used to derive order-of-magnitude estimates for the characteristics sizes and ranges of these offsets, $\Delta E \sim \epsilon$ and $\Delta J \sim j$, where

$$\epsilon = r_{\text{tide}} \left(\frac{d\Phi}{dR} \right)_{R_p} = s \frac{GM_p}{R_p} \quad (4)$$

and

$$j = sJ. \quad (5)$$

Given these characteristic ranges, the angular length of streams of debris as viewed from the Galactic center is expected to grow by of order

$$\Delta\Psi = \epsilon \left[\frac{2\pi}{T_\Psi} \frac{dT_\Psi}{dE} \right]_{J=J_{\text{circ}}}, \quad (6)$$

each orbit, where J_{circ} is the angular momentum of a circular orbit of energy E and azimuthal time-period $T_\Psi(E)$ at radius $R_{\text{circ}}(E)$. The secondary dependance of orbital time periods on angular momentum has been ignored. The angular width is initially of order

$$w = s. \quad (7)$$

and is expected to grow with time at a rate dependent on the parent potential (Helmi & White 1999). For near-spherical potentials the rate is sufficiently small that the approximation $w \sim s$ remains useful for many orbits (Johnston et al. 2001).

2.3. The case of Palomar 5

Tidal streams associated with the globular cluster Palomar 5 were discovered using SDSS data by Odenkirchen et al. (2001, 2003) stretching several degrees away either side of the center of the cluster, and have now been mapped to a total extent of 22 degrees (Grillmair & Dionatos 2006a). They were the first debris to be mapped from such a small object and remain a primary example of a thin, cold stream.

The first set of rows of Table 1 list the observed characteristics of Pal 5's stream. Since Pal 5's orbit is not much further from the Galactic center than the Sun, these are roughly translated into a Galactocentric view in the second set of rows, assuming the Sun is at 8 kpc from the Galactic center — for example, a lower limit on the Galactocentric angular length is taken to be $l = (D_{\text{debris}}/R_{\text{debris}})l_{\text{obs}}$ where D_{debris} and R_{debris}

Object	Pal 5	Sgr
Heliocentric view		
D_{debris} (kpc)	~ 23.5	8-80
w_{obs} (degrees)	0.5	10
l_{obs} (degrees)	22	> 360
Galactocentric view		
R_{debris} (kpc)	18	8-80
l (degrees)	> 29	> 360
assumed properties		
R_p (kpc)	7.5	15.0
R_a (kpc)	19.2	60.0
T_R (Gyrs)	0.33	0.89
T_Ψ (Gyrs)	0.55	1.35
R_{circ} (kpc)	13.7	40.1
$m_{\text{sat}} (M_\odot)$	10^4	5×10^8
age (Gyrs)	8.44	1.9
derived scales		
s	0.007	0.17
ϵ (km/s) ²	123	4572
$\Delta\Psi$ (degrees)	1	42
w (degrees)	0.4	10

Table 1

Properties of the Pal 5 and Sgr streams.

are the heliocentric and Galactocentric distances respectively. The observed properties can be broadly reproduced with an N-body simulation of a hot, spherically symmetric system disrupting along an orbit with characteristics listed in the third set of rows (“assumed properties”) of Table 1. The simulation adopted a 10,000-particle Plummer model with mass $10^4 M_\odot$ and scale length 7.5 pc for Pal 5, and calculated its self-gravity using Hernquist & Ostriker (1992) “self-consistent-field” code. The model was allowed to evolve in the NFW parent potential described in Section 2.1 for 8.44 Gyrs. Very similar masses and orbits were found with the more extensive modeling by Dehnen et al. (2004).

The left-hand panels of Figure 2 summarize the results of our simulation. The top left-hand panel shows the energy-angular momentum distribution of debris particle, with axes scaled by the factors given by equations (4) and (5), and listed in the bottom set of rows in Table 1. Note that debris particles are systematically offset from those still-bound to the satellite, and distributed in the range $\pm 3\epsilon$ and $\pm 3j$ around the satellite’s own orbital energy/angular-momentum — a result that is found to be largely independent of satellite mass, scale, profile and orbit (e.g. Johnston 1998). Note that the range in scaled-angular-momenta does depend (mildly) on the eccentricity of the orbit, with debris on more eccentric orbits exploring larger ranges.

The bottom left-hand panel of Figure 2 shows the final position of the particles projected onto the plane of the sky, as viewed from a Solar position in our model. From our assumed mass and orbit, our analytic estimate (i.e. equation 7) suggests an angular width $w \sim 0.4$ degrees for the debris. While this is of the same order as both the observed and simulated width, this prediction is relatively insensitive to the assumed mass for the satellite, so the agreement should only be seen as a weak confirmation that the mass of the satellite is the correct order of magnitude.

The estimated angular length of a stream of age t

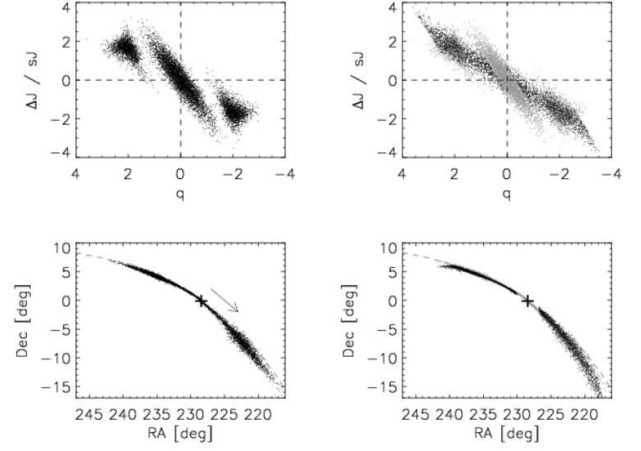


Figure 2. Different representations of the globular cluster, Pal 5. N-body (left hand panels) and test particle streams (right hand panels) shown in energy/angular-momentum space (top panels) and in the sky (bottom panels). The dashed lines in the top panels show the mean orbital properties adopted for the test-particle streams. In the right-hand panels, the gray dots repeat the N-body results from the left and the black dots are the test particles. The dashed lines in the bottom panels represent the orbital path and the arrow shows the direction of the moving stream.

viewed from the Galactic center is

$$l = 4 \frac{t}{T_\Psi} \left(\frac{R_{\text{circ}}}{R_{\text{debris}}} \right)^2 \Delta\Psi, \quad (8)$$

where $\Delta\Psi$ is the expected angular growth per orbit calculated from equation (6) for the given mass and orbit. The additional scaling, dependent on the radial phase at which the debris is observed (i.e. distance of debris from the Galactic center R_{debris}), is included to account for the effect of debris density increasing/decreasing as the angular speeds decrease/increase ($\propto (1/R_{\text{debris}})^2$ in a spherical potential from conservation of angular momentum. The extra factor of 4 reflects the range that characterizes the width of the energy distribution seen in the top left-hand panel of Figure 2 (i.e. $\pm 2\epsilon$). The prediction for the angular length of the stream, as observed from the Solar position, is given by

$$l_{\text{obs}} = \left(\frac{R_{\text{debris}}}{D_{\text{debris}}} \right) l. \quad (9)$$

For the parameters adopted in our simulation of Pal 5 we find $l_{\text{obs}} \sim 30$ degrees, which agrees with the length seen in the lower-left panel of Figure 2.

2.3.1. Initial Conditions for Numerical Experiments

This paper employs a simplified representation of N-body results that characterizes the evolution of tidal debris described above using test particles integrated in the combined potential of the parent and orbiting lumps, but ignoring the self-gravity of the satellite. The particles are given initial positions and velocities slightly offset from the satellite’s own, that are chosen to reproduce the scaled energy and angular momentum distributions seen in the top left-hand panel of Figure 2. Specifically, the particles are initially positioned uniformly distributed

along two lines pointing in the direction of the Galactic center and centered on the satellite at the apocenter of its orbit at Galactocentric radius $R = R_a$ and tangential velocity v_{tan} . Particles at position ΔR along the bars relative to the satellite are assigned a tangential velocity $v_{\text{tan}} + \Delta v$, where these offsets in position and velocity satisfy the equations:

$$\begin{aligned}\Delta E &= \alpha \epsilon = v_{\text{tan}} \Delta v + \Delta R \left(\frac{d\Phi}{dR} \right)_{R=R_a} \\ \Delta J &= \beta j = v_{\text{tan}} \Delta R + R \Delta v.\end{aligned}\quad (10)$$

Here α is restricted to the range ± 3 and $\beta = 2.5\alpha/3$ in order to mimic range in the orbital properties seen in the simulations. In addition, the particles are assigned small random velocities in the x , y and z directions around the mean $v_{\text{tan}} + \Delta v$ chosen from a gaussian with width $\sigma = 0.6sv_{\text{tan,apo}}$ to reproduce the spread in angular momentum at a given energy.

The right-hand panels of Figure 2 illustrate the success of this method by comparing energy/angular-momentum distributions (top panel) and final positions (bottom panel) for our N-body (gray particles) and test particle (black points) model of debris evolution for Pal 5 (assumed properties in third set of rows of Table 1).

3. RESULT I: ANALYTIC ESTIMATES

In this section we use simple analytic arguments to derive order-of-magnitude estimates for the frequency of encounters of streams with varying mass dark-matter substructures (§3.1) and the characteristic scales of these subhalos' influence on the debris (§3.2). We first illustrate the implications of these estimates for the debris from Pal 5 and then go on to discuss the application to other streams (§3.3).

3.1. Frequency of Encounters

Suppose a (perfectly tubular!) stellar stream of angular length l and angular width w is orbiting at an average distance R_{circ} from the Galactic center through a sea of dark-matter subhalos of size r_{tidal} and number density n_{subhalo} . The rate of encounters that directly impact the stream with relative speeds in the range $(v, v + dv)$ can be estimated as:

$$\begin{aligned}\frac{dN_{\text{enc}}}{dt} &= \text{volume encounter rate} \times \text{number density} \times P_{\text{rel}}(v)dv \\ &= (\text{stream surface area}) \times v \times n_{\text{subhalo}} \times P_{\text{rel}}(v)dv \\ &= (R_{\text{circ}} l \times 2\pi b_{\text{max}}) \times n_{\text{subhalo}} \times v P_{\text{rel}}(v)dv.\end{aligned}\quad (11)$$

where $P_{\text{rel}}(v)$ is the probability distribution of relative speeds. The maximum impact parameter for direct encounters is taken from the condition that the stream and subhalo overlap physically:

$$b_{\text{max}} = \text{MAX}[wR_{\text{circ}}/2, r_{\text{tidal}}]. \quad (12)$$

Assuming that the local velocity distribution of the subhalos is an isotropic Maxwellian with dispersion σ , we can approximately represent the relative distribution of encounter speeds along a typical orbit by the relative speed distribution between the subhalos

$$P_{\text{rel}}(v)dv = \frac{1}{(\sqrt{2\pi}\sigma)^3} v^2 \exp\left(-\frac{v^2}{4\sigma^2}\right) dv \quad (13)$$

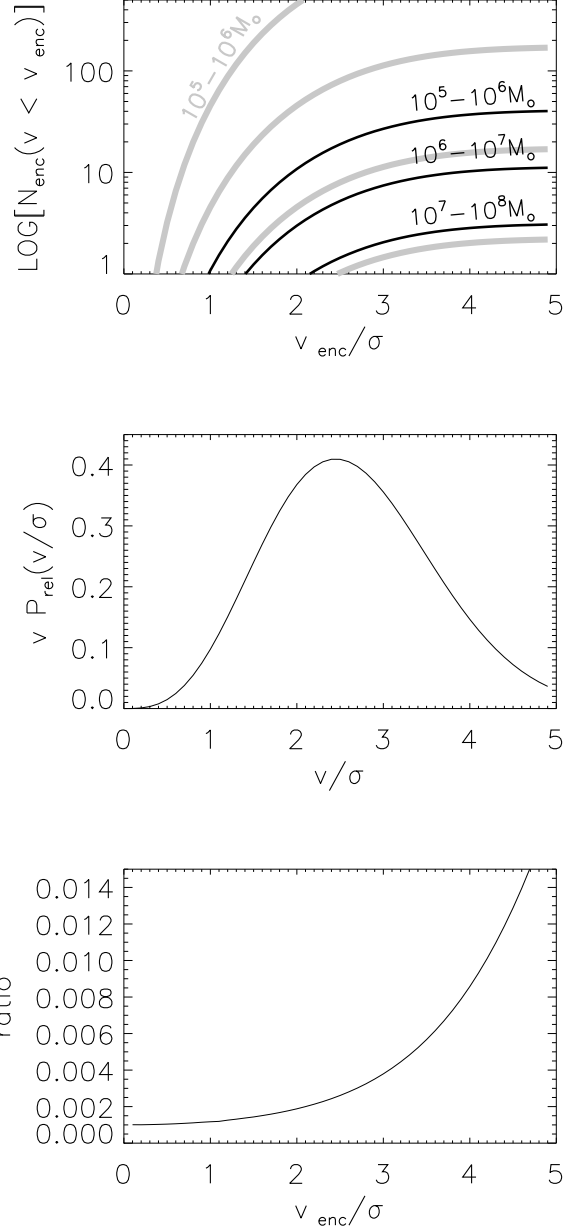


Figure 3. Encounter frequencies. The upper panel plots the estimated number of direct encounters for Pal 5 (solid lines) and Sgr (gray lines) debris during the debris lifetime and for subhalos of different masses. Each line presents the case for different subhalo mass decades as noted on the lines. The middle panel shows the distribution of encounter velocities. The bottom panel shows an estimate for the fraction of encounters of fixed energy that are due to slow encounters with small masses (see text).

(see Binney & Tremaine 2008, equation (8.46)). This implies a typical encounter speed of

$$v_{\text{enc}}^{\text{typ}} = \frac{\int_0^\infty v^2 P_{\text{rel}}(v) dv}{\int_0^\infty v P_{\text{rel}}(v) dv} = 3\sqrt{\pi}\sigma/2. \quad (14)$$

Replacing l in equation (11) with equation (8) (evaluated for $R_{\text{debris}} = R_{\text{circ}}$) and integrating over speeds and time, we find the number of encounters with encounter

speeds less than v_{enc} that this stream experiences over its lifetime t :

$$N_{\text{enc}}(v < v_{\text{enc}}) = 8\sqrt{\pi} R_{\text{circ}} b_{\text{max}} \sigma t n_{\text{subhalo}} \times \Delta\Psi \left(\frac{t}{T_{\Psi}} \right) \times \left[1 - \left(1 + \frac{v_{\text{enc}}^2}{4\sigma^2} \right) \exp \left(-\frac{v_{\text{enc}}^2}{4\sigma^2} \right) \right] \quad (15)$$

The solid lines in the top panel of Figure 3 show $N_{\text{enc}}(v < v_{\text{enc}})$ for our Pal-5-like stream (i.e. evaluating equation 15 with parameters adopted from Table 1) as a function v_{enc} for different decades in subhalo masses and assuming a characteristic σ of 120 km/s. (Note that the circular velocity at radius 25 kpc in a spherical NFW halo with parameters chosen to match the parent halo in VLII is 178 km/s, which suggests a dispersion of $178/\sqrt{2}=126$ km/s.) The subhalos in each group are assumed to have tidal radii similar to those seen in VL II for subhalos within 25kpc (i.e. $r_{\text{tidal}} = 0.21, 0.58, 1.6, 4.5, 12.7$ kpc for masses in ranges $10^5 - 10^6/10^6 - 10^7/10^7 - 10^8/10^8 - 10^9/10^9 - 10^{10}M_{\odot}$ respectively — see Figure 1). For n_{subhalo} we adopt the mean number density within 25 kpc given by assuming there to be 42 subhalos in the range $10^6 - 10^7 M_{\odot}$ within this volume (as seen in VLII, see Figure 1), and a factor of 10 more/less in each subhalo mass decade below/above (to mimic the mass spectrum seen in VLII). (This is expected to be an upper limit on the number of encounters since the adopted age produces a stream slightly longer than the observed stream, and the mass adopted for our Pal 5 model was fairly low.) Inserting these numbers for the $10^6 - 10^7 M_{\odot}$ mass range explicitly into equation 15 and letting $v_{\text{enc}} \rightarrow \infty$ gives the total number of direct encounters:

$$N_{\text{enc, total}}(M_{\text{sub}} = 10^6 - 10^7 M_{\odot}) = 11 \left(\frac{R_{\text{circ}}}{13.7 \text{ kpc}} \right) \times \left(\frac{b_{\text{max}}}{0.58 \text{ kpc}} \right) \left(\frac{\sigma}{120 \text{ km/s}} \right) \left(\frac{t}{8.44 \text{ Gyrs}} \right)^2 \times \left(\frac{n_{\text{subhalo}}}{0.0006 \text{ kpc}^{-3}} \right) \left(\frac{\Delta\Psi}{1^{\circ}} \right) \left(\frac{0.55 \text{ Gyrs}}{T_{\Psi}} \right) \quad (16)$$

Overall, our calculations indicates that Pal 5's stream will have suffered hundreds of direct encounters with subhalos less massive than $10^5 M_{\odot}$, ~ 40 with subhalos masses in the range $10^5 - 10^6 M_{\odot}$, tens with subhalos of $10^6 - 10^7 M_{\odot}$ and a few with subhalos of $10^7 - 10^8 M_{\odot}$. Subhalos in the higher mass bins are very unlikely to directly hit the stream, although they will influence it through more distance encounters. In addition, note that while there are sufficient numbers of smaller subhalos to fully explore the relative velocity distribution, the few encounters with large subhalos are likely to take place close to the typical encounter speed around the peak of the velocity distribution shown in the second panel.

3.2. Effect of Encounters

In order to develop some understanding of the effect of subhalos on streams, consider the idealized case of a subhalo encountering a perfectly straight stellar stream aligned with the x -axis, with impact parameter b along

the y -axis and relative velocity $\mathbf{v}_{\text{enc}} = (v_x, 0, v_z)$. Overall, the change in speed of the stars perpendicular to the stream is zero by symmetry. Assuming the change in the relative speed for stars in the stream is negligible during the encounter ($\Delta v_x \ll v_x$) and simply integrating the equations of motion we find

$$\begin{aligned} \Delta v_x &= \int_{-\infty}^{\infty} a_x dt \\ &= \int_{-\infty}^{\infty} \frac{GM_{\text{sub}}(v_x t + x)}{[(v_x t + x)^2 + b^2 + v_z^2 t^2]^{3/2}} dt \\ &= -\frac{2GM_{\text{sub}}x}{v_{\text{enc}} b^2} \frac{v_z^2}{v_z^2 (x/b)^2 + v_{\text{enc}}^2} \end{aligned} \quad (17)$$

where x is the position of the star in the stream at the moment of closest approach of the subhalo, relative to the impact point. If the space motion of the stars in the streams in the Galactic rest-frame is v_{stream} , then the energy change is

$$\Delta E = \mathbf{v}_{\text{stream}} \cdot \Delta \mathbf{v} + \frac{1}{2} \Delta v^2 = v_{\text{stream}} \Delta v_x + O(\Delta v_x^2) \quad (18)$$

For direct encounters with subhalos of mass M_{sub} :

$$\Delta E(b=0) = 2 \frac{GM_{\text{sub}}}{x} \frac{v_{\text{stream}}}{v_{\text{enc}}}. \quad (19)$$

3.2.1. Lowest Mass Subhalos

Figure 3 suggests Pal 5 experiences thousands of encounters with subhalos less massive than $10^5 M_{\odot}$ during its lifetime. In this many, weak encounter regime the first term in equation (18) should average out to zero and leave the second term to heat the stellar stream. Despite their large number, since the heating term is second order, these encounters would have negligible effect compared to the few encounters with larger subhalos. For example, while there would be a factor of ten more encounters with $M_{\text{sub}} \sim 10^4 - 10^5 M_{\odot}$ than in the mass decade above, the net energy change due to each of those encounters would be a factor of 100 smaller, so the individual encounters with larger lumps would be generally be expected to have a more significant effect.

Nevertheless, equation (19) indicates that the effect of a lower mass subhalo can be comparable to that of a subhalo in the mass decade above if the encounter with the lower mass is ~ 10 times slower. Indeed, the large number of encounters with low mass halos ensures that a small number will come from the low-end stream of the relative velocity distribution (see middle panel of Figure 3) and the effect of these few, slow encounters would not be expected to average out. The lower panel of Figure 3 compares the frequency of these *slow* encounters with low mass subhalos relative to ones of comparable influence in the mass decade above by plotting the ratio of the number of encounters of low mass subhalos to higher mass subhalos of comparable influence: $[10N_{\text{enc}}(v < v_{\text{enc}}/10)]/N_{\text{enc}}(v < v_{\text{enc}})$. Since this ratio is never much greater than 1% we conclude that while rare, influential low-speed encounters with low mass subhalos can occur, they will be much less frequent than encounters of comparable influence with higher-mass subhalos.

3.2.2. Intermediate Mass Subhalos

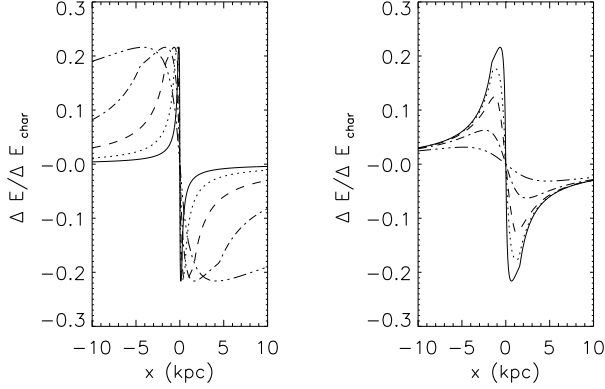


Figure 4. Estimate for the scaled energy imparted by a direct encounter at $x = 0$ at different points along a stream. The left hand panel shows the influence of subhalos of mass $5 \times 10^5/5 \times 10^6/5 \times 10^7/5 \times 10^8/5 \times 10^9 M_\odot$. The right hand panel plots the result for a subhalo of mass $5 \times 10^7 M_\odot$, traveling perpendicularly to the stream and with impact parameters $b = 0/2/4/8/16 r_s$.

Pal 5 should have experienced ~ 10 direct encounters with subhalos in the mass range $10^6 - 10^7 M_\odot$, whose influence is unlikely to average to zero. In order to gain some intuition for their effect, the left hand panel of Figure 4 plots equation (19) for values for the stream and encounter speeds averaged over their respective velocity distributions ($v_{\text{stream}}^{\text{typ}} = 2\sqrt{2/\pi}\sigma$ and $v_{\text{enc}}^{\text{typ}} = 3\sqrt{\pi}\sigma/2$) and $M_{\text{sub}} = 5 \times 10^5/5 \times 10^6/5 \times 10^7/5 \times 10^8/5 \times 10^9 M_\odot$ (solid...dot-dot-dot-dash lines), as a function of position x along the stream. The extended nature of these subhalos was taken approximately into account by replacing M_{sub} in equation (17) with the mass enclosed within radius $r = x$ for an NFW model with scale r_s ($M_{\text{sub}}(r)$). (Note that the integral was solved analytically and did not take this into account). The subhalos had r_s chosen to match those within 25kpc in VLII ($r_s = 0.05, 0.12, 0.30, 0.76, 1.94$ kpc respectively). In order to show the behavior of ΔE for these different mass ranges in a single plot, the energy change was normalized by the characteristic energy for a direct encounter, calculated by substituting $x = r_s$ in equation (19):

$$\Delta E_{\text{char}} = 2 \frac{GM_{\text{sub}} v_{\text{stream}}^{\text{typ}}}{r_s v_{\text{enc}}^{\text{typ}}} = \frac{8\sqrt{2}}{3\pi} \frac{GM_{\text{sub}}}{r_s}. \quad (20)$$

Most noticeable in Figure 4 is the abrupt sign-change in ΔE at the impact point — stars upstream of the impact point are pushed to orbits of higher energy and stars downstream of the impact point are pushed in the opposite direction to orbits of lower energy. This effect exaggerates the energy gradient already present along the stream (see §2.2) and creates a gap in energy. The fraction of the stream affected by the encounter depends on the size of the perturber — with the smallest subhalos influencing only a subset of stream particles directly around the impact point (solid lines) and the largest subhalos influencing the whole stream (triple-dot-dashed line).

How influential these encounters are on debris evolution also depends on stream characteristics. The top and middle panels of Figure 5 assess this by plotting ΔE_{char}

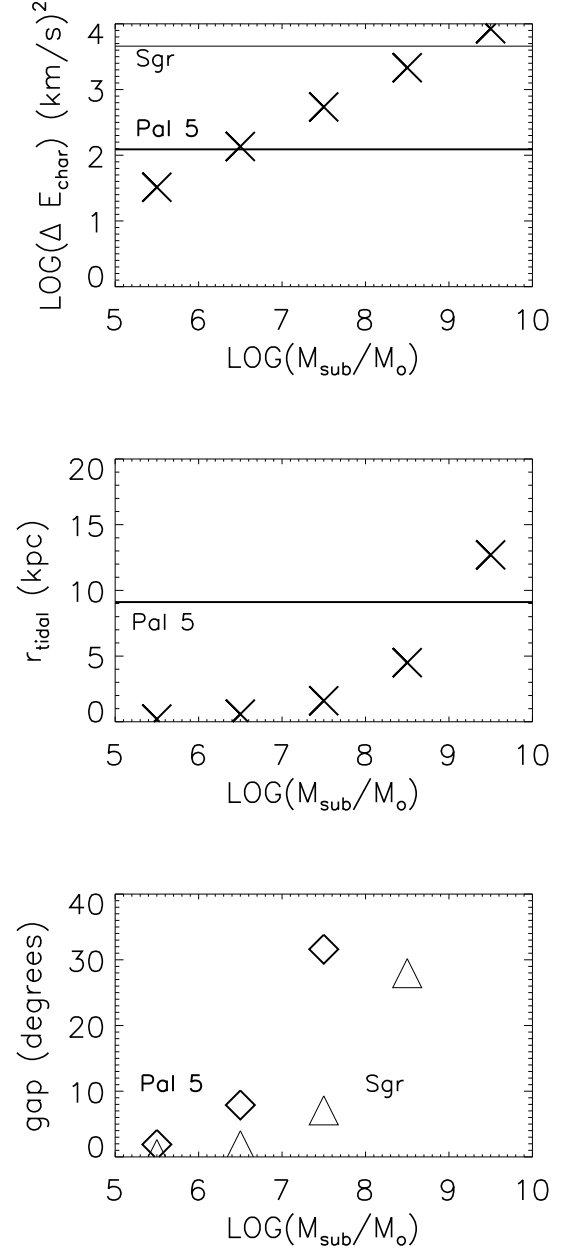


Figure 5. Scales in an encounter relative to stream properties for subhalos of different masses. The top panel compares ΔE_{char} (symbols) with the intrinsic energy spread in Pal 5's (bold line in the middle) and Sgr's (faint line on the top) debris. The middle panel compares the length of Pal 5's stream with the tidal radius of the subhalos (Sgr's stream is far longer than the plot). The lower panel gives an upper limit on the angular scales of gaps due to encounters with Pal 5 (bold diamond symbols) and Sgr (faint triangle symbols) debris.

for subhalos of different masses and the spatial scale over which this energy change is important (taken to be the tidal radius r_{tidal}). For comparison, the energy scale over which debris orbits are spread for Pal 5 (i.e. ϵ , calculated from equation 4) and the physical length of the stream itself are shown as bold lines. These plots suggest that each direct encounter of Pal 5's debris with subhalo masses in

the range $10^6 - 10^7 M_\odot$ should create gaps in energy that are a significant fraction of the spread of energy already present in the debris (i.e. $\Delta E_{\text{char}} \sim \epsilon$) for of order 10% of stars in the stream (i.e. $r_{\text{tidal}} \sim l/10$).

Over time these gaps in energy will cause the stream stars around the impact point to spread apart from each other faster than stars in other regions of the stream, leading to physical gaps in the stream density distribution. We can estimate an upper limit on the angular scale of these physical gaps by replacing the stream energy range 4ϵ in equation (8) with ΔE_{char} and calculating l_{obs} for Pal 5's lifetime and orbit (assumed parameters in Table 1). The bold diamonds in the lower panel of Figure 5 show this estimate.

Overall, we conclude that direct encounters of Pal 5's debris with subhalo masses in the range $10^6 - 10^7 M_\odot$ during its lifetime could lead to tens of gaps in density of order several degrees across, while masses in the range $10^5 - 10^6 M_\odot$ could leave many more on sub-degree scale. Few, if any, direct encounters are likely to occur for the Pal 5 stellar stream for masses greater than $\sim 10^7 M_\odot$ (as shown in Figure 3), but could potentially lead to larger gaps.

3.2.3. Indirect Encounters with Largest Mass Subhalos

The right hand panel of Figure 4 repeats the same plot as the left hand panel, but this time for a $10^7 M_\odot$ subhalo traveling perpendicularly to the stream (i.e. $v_{\text{enc}} = v_{\text{enc}}^{\text{typ}} = v_y$) and passing it at impact parameters b of 0, 2, 4, 8, 16 r_s . Note that for these more distant encounters the impulsive approximation under which equation (17) was derived breaks down and the estimate is likely to overestimate the size of a subhalos' influence. The results are nevertheless included here as a broad guide to general behavior, but should be treated with some skepticism. The effect of more distant encounters can be assessed more realistically using numerical integration (see §4).

As the impact parameter increases, both the size of the energy change decreases and the scale over which it is felt grows. The energy imparted to the stream changes more smoothly as a function of position along the stream than in the direct encounter case, with the most extreme changes apparent at the edges. This is in part because the impact parameter is now comparable to the length of the stream itself and it is only at the edges that the velocity change is aligned with the stream velocity to produce maximum energy change. The net result is that the stream is smoothly stretched in energy, rather than forming an abrupt gap. It is this type of interaction that dominates for the larger masses: Figure 3 tells us we should expect few such encounters over Pal 5's lifetime.

Note that the same behavior can be seen for individual encounters for smaller masses, but in those cases there are sufficient numbers of weak encounters for the first-order terms in energy change to cancel out. So we conclude that indirect encounters of smaller masses are not important for leaving observable signatures.

3.3. Summary and Application to Other Streams

In summary, our analytic estimates indicate that Pal 5's stream should be sensitive to dark subhalos, with unique signatures from different subhalo masses. The

dominant influence on streams like Pal 5's will be from scattering of stars by encounters with subhalos in the mass decades $10^5 - 10^7 M_\odot$ where a few to many tens of encounters occur during the stream's lifetime. These events will lead to gaps in the stream with characteristics scales reflecting the mass of the perturbers. Low-speed encounters from smaller subhalos can create comparable gaps, but these events occur much less frequently and so should not confuse the signal. Heating by perturbers in the lower mass decades should also be negligible. Direct encounters with larger masses are unlikely (though catastrophic if they occur), and indirect encounters will tend to stretch rather than chop up a stream.

Our estimates also suggest that streams with Pal 5's scales are the most interesting. The thin lines and symbols in Figure 3 illustrate the results of repeating the calculations made above for Pal 5's stream for Sgr's debris. In comparison to Pal 5, these streams have a far larger cross section for encountering dark-matter subhalos, but also have a far larger spread in orbital properties in which to hide the signatures of encounters. This means that the influence of encounters with subhalos less massive than $10^8 M_\odot$ are likely to be negligible as: (i) both the spatial and energy scales of the change are much smaller than the inherent stream scales (see first and second panels of figure 5), and (ii) the encounters become frequent enough that first order changes may be expected to cancel out. Subhalos more massive than $10^8 M_\odot$ could leave their imprint on Sgr debris. However, these dark-matter structures are generally thought to contain stars and hence should be detectable by other means.

We conclude that for the purposes of finding *missing* satellites, cold streams from low mass objects should be the most sensitive probes.

4. RESULT II: NUMERICAL ILLUSTRATIONS

This section presents the results of scattering test particle streams by subhalos with numerical integration. We present our results in orbital (i.e. energy/angular-momentum) space, coordinate space, and observable space. The Sun is assumed to be at $(X, Y, Z) = (-8\text{kpc}, 0, 0)$.

In the following subsections, we look first at individual close encounters (§4.1), then multiple encounters for subhalos in each mass decade (§4.2), and finally examine the combined effect of all subhalos in the full Λ CDM mass spectrum (§4.3).

4.1. Individual Encounters

We first follow a single artificial encounter with $M_{\text{sub}} = 10^{6.5} M_\odot$, $r_s = 0.118\text{kpc}$ and $r_{\text{tidal}} = 0.590\text{kpc}$ passing directly through a Pal 5-like stream perpendicular to the orbital plane with a relative velocity $(v_x, v_y, v_z) = (0, 0, -200\text{km/s})$ to the stream. Figure 6 illustrate the effect of this direct encounter on the stream (fiducial results in each panel labelled with (f)). The orbital plane of the stream is in the X-Y plane. The left column shows the moment of closest approach of the subhalo encounter moving along the z-direction and passing perpendicularly through the stream. The middle and right columns show the particle positions in the X-Y and energy/angular-momentum planes 4.34 Gyr after the encounter. There is a clear energy gap around the impact point in the stream

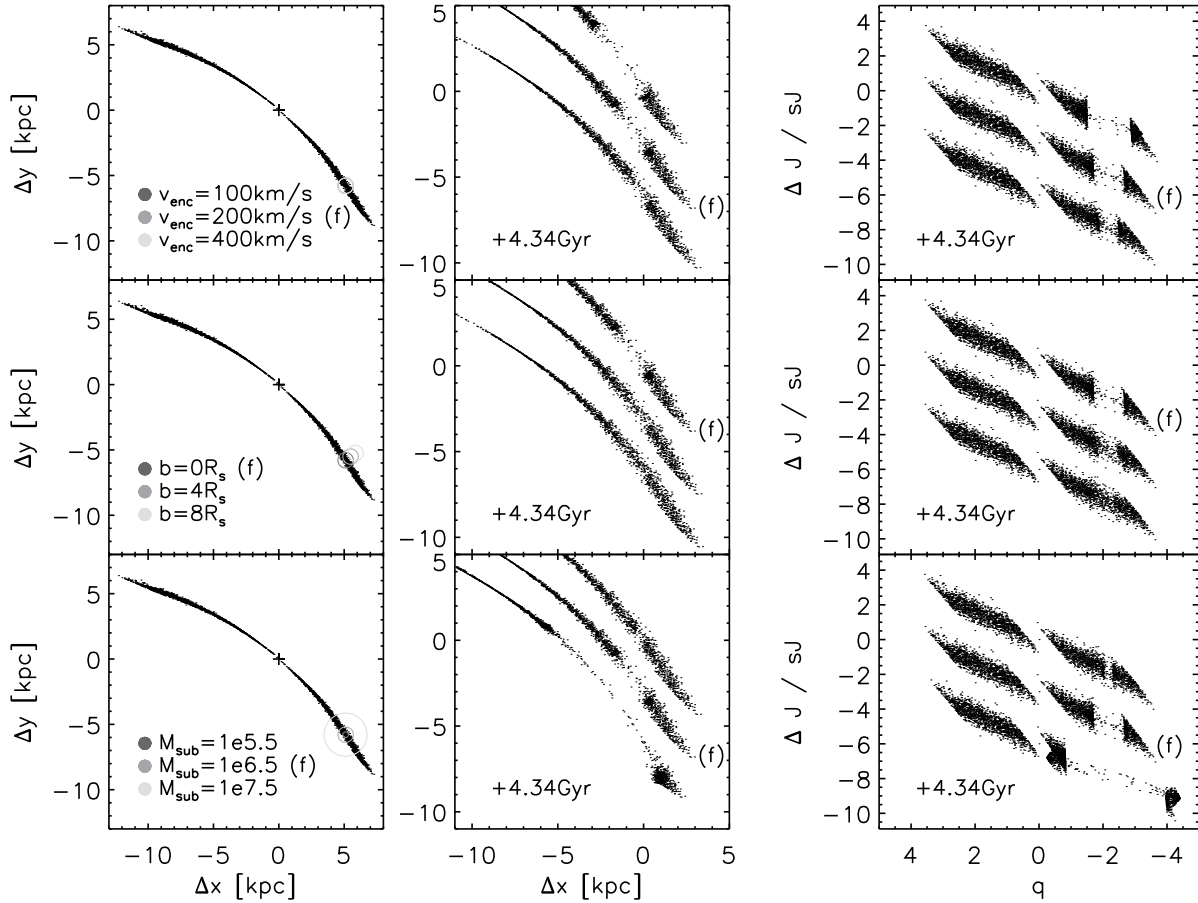


Figure 6. The various effects of encounters on a Pal 5-like stream. Our fiducial encounter (particles labelled *(f)* in each panel) has $M_{\text{sub}} = 10^{6.5} M_{\odot}$, $v_{\text{enc}} = 200 \text{ km/s}$, $b = 0$. The top/middle/bottom rows show the responses when the velocity/impact/mass are allowed to vary around this. The “+” in each panel represents the Pal 5 center, and the circles show the size (r_{tidal}) of the encounters and where they pass through. Note that three encounters are all overlapped in the top-left panel. The streams in the first, second, and last columns are centered at the Pal 5 center, impact point, and mean energy/angular-momentum respectively. Streams other than the fiducial model are shifted by -3 and -6 along y-axis from their original positions in the second and last columns.

that forms immediately after closest approach: the particles behind the impact points (with higher energy) are accelerated (gain energy) and the ones ahead the impact points (with lower energy) are decelerated (lose energy) as predicted in §3.2.2. This energy gap results in a spatial gap along the stream which grows with time due to phase mixing as illustrated in the middle column. Hence, a stream influenced by many encounters should end up having a clumpy structure produced by numerous energy and spatial gaps.

Having illustrated the nature of the gaps in energy, we now investigate how these response of the stream to varied encountering conditions. The first row of Figure 6 illustrates the effect of encounters with different velocities relative to the stream ($v_{\text{enc}} = 100, 200, 400 \text{ km/s}$), the second row shows the gaps resulting from encounters passing with different impact parameters ($b_{\text{impact}} = 0 \times, 4 \times, 8 \times r_s$ which correspond to 0, 0.470, 0.940 kpc), and the last row shows various mass encounters ($M_{\text{sub}} = 10^{5.5}, 10^{6.5}, 10^{7.5} M_{\odot}$). Overall, when the velocity of the encounter doubles the gap becomes half, while smaller impact parameters and larger masses result in larger en-

ergy gaps. These scalings agree with the trends in the equations (17), (18), and (19). For a stellar stream orbiting with many dark matter subhalos, irregular clumps are expected in the stream that correspond to various energy gaps created by different encounters at different times.

Lastly, the bottom panels suggest that while a small subhalo has an effect on the local region of a stream generating a small energy gap, a close encounter with a subhalo larger than $10^{7.5} M_{\odot}$ can globally distort the entire energy-angular momentum scales, since the size and influence of the subhalos are larger than the entire stream. This will be discussed in more detail in § 4.2.

4.2. Multiple Encounters

To examine the integrated influences of many subhalos, we perform separate simulations with subhalos drawn from each decade of the Λ CDM mass spectrum. We first illustrate our results by contrasting simulations with the $\sim 30,000$ intermediate mass subhalos in the mass range $10^6 - 10^7 M_{\odot}$ and ~ 30 large mass subhalos of $10^9 - 10^{10} M_{\odot}$. Figure 7 shows the final spatial and

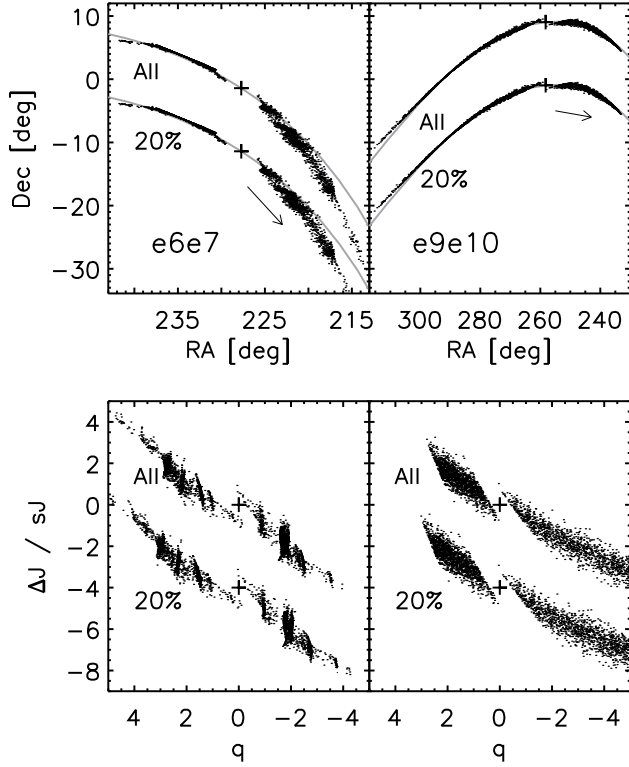


Figure 7. The final distribution of stream particles from simulations of encounters with all the subhalos (upper particle distributions) and the 20% closest encounters (lower particle distributions) in the mass range $10^6 - 10^7 M_\odot$ (left panels) and $10^9 - 10^{10} M_\odot$ (right panels). The top row shows the stream in the sky and the bottom row shows the energy/angular-momentum distribution. The arrows illustrate the direction of the stream movement and the cross represents the center of host satellite Pal 5. The grey lines illustrate the orbits of satellites. The lower particles have been shifted for clarity by -10° and by -4 along the y-axis in the top and bottom panels respectively.

energy/angular-momentum distribution of these cases. First consider the overall morphologies in Figure 7. Recall that the calculation in §3.1 suggests there should be ~ 10 direct encounters with subhalos in the lower mass range, which is in rough agreement with the visual impression of the energy/angular-momentum distribution in the lower left-hand panel. In contrast, the stream with the large subhalos (the right column of Figure 7) does not have any gaps. Instead, the orbital phase of the stream with subhalos in the mass range $10^9 - 10^{10} M_\odot$ is shifted and the entire energy scale is changed as suggested in § 4.1. All panels in Figure 7 are plotted relative to a central particle (marked with +). The scaled energy q and angular momentum ($\Delta J/sJ$) values of the central particles changed by $(-0.74, -0.53)$ and $(9.40, 4.00)$ for the streams with $10^6 - 10^7 M_\odot$ and $10^9 - 10^{10} M_\odot$ subhalos respectively. This phase and energy shift will not be observable since there is no way to probe the original phase and energy.

In order to disentangle the effect of direct (close) encounters from indirect (distant) ones, we select the 20% closest encounters based on the minimum distance between the subhalos and the stream particles that occurs

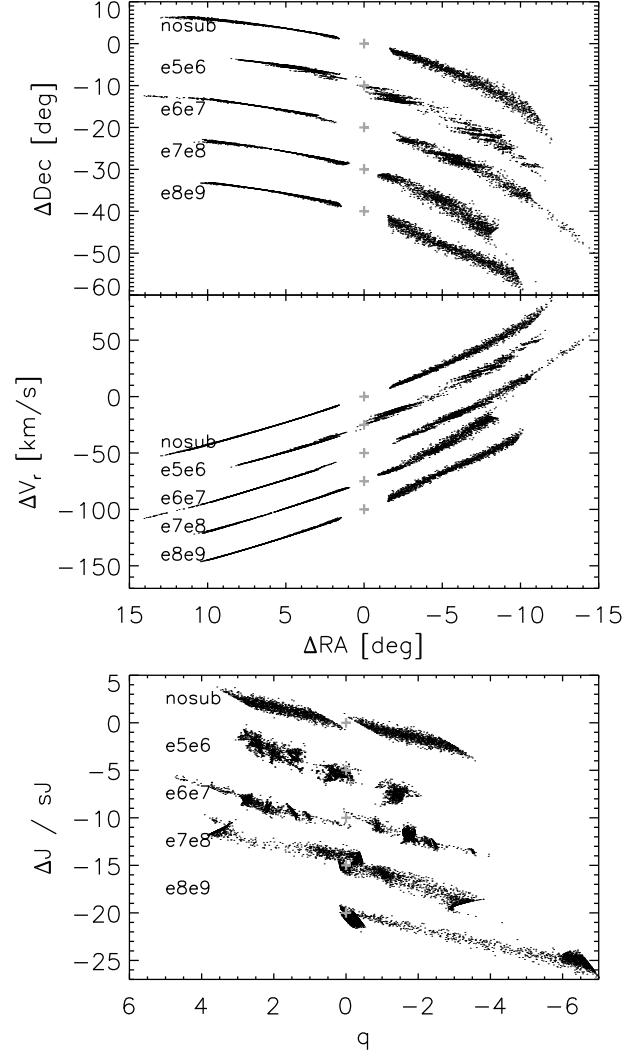


Figure 8. Final distribution of stream particles from simulations with subhalo encounters of varying mass ranges. The streams with no subhalos, subhalos in the mass range $10^5 - 10^6 M_\odot$, $10^6 - 10^7 M_\odot$, $10^7 - 10^8 M_\odot$, and $10^8 - 10^9 M_\odot$ are shown in the sky (top), radial velocity (middle), and energy/angular-momentum space (bottom). The stream with no subhalos is at the original position and the others are shifted down by 10 and 5 for the top and bottom panel respectively. The grey crosses represent the center of the host satellite.

throughout the simulations. We then re-run the same simulation with only these subhalos present. The results, presented in the lower particle distributions in each panel of Figure 7, are almost identical to the ones with all subhalos in each mass range, which suggest that heating by the more distant encounters is negligible.

Figure 8 repeats the plots in Figure 7 for simulations with subhalos in all mass decades. While the stream without any subhalos shows a smooth morphology in the sky and energy/angular-momentum space, the streams with subhalos in the mass range $10^5 - 10^6 M_\odot$, $10^6 - 10^7 M_\odot$, and $10^7 - 10^8 M_\odot$ show eye-catching signatures such as spatial, velocity, and energy gaps. As expected, the smaller subhalos cause many more smaller scale clumps in the stream than the large ones. In con-

trast, the stream with $10^8 - 10^9 M_\odot$ subhalos does not have clear signatures. These subhalos are too large to leave small scale variations but too small to shift the entire stream as in Figure 7. Rather, these subhalos distort the energy-angular momentum distribution and slightly change the overall shape of the stream.

The gaps in Figure 8 due to $10^5 - 10^6 M_\odot$ subhalos are more commonly smaller than those due to the $10^6 - 10^7 M_\odot$ objects. This indicates that each mass decade might be separately detected. While small encounters with subhalos will generally result in smaller energy gaps which correspond to smaller physical gap than encounters with large subhalos, note that in the middle of the leading part of the stream with $10^5 - 10^6 M_\odot$ subhalos, there is a large gap (where $\Delta RA \sim -5^\circ$) which is as big as the ones in the stream with $10^6 - 10^7 M_\odot$ subhalos. On further investigation, we found this large gap can be attributed to a very slow encounter (which caused a large gap in energy) that occurred relatively early in the simulations (which allowed the gap to grow). However, we expect this to be a rare occurrence as described in §3.1. To confirm this expectation, we ran four additional simulations with the same conditions as the original $10^5 - 10^6 M_\odot$ run but different initial starting points. In none of these cases did such large gaps appear.

We can also extrapolate from these numerical results to consider the effect of the smallest “missing satellites” with $M_{\text{sub}} < 10^5 M_\odot$. The scales of the gaps due to individual encounters with these subhalos will be even smaller than those due the mass decade above (like the ones apparent in Figure 8) and would thus require a very high resolution map to detect. Making such a map is observationally challenging since Pal 5’s stream contains only a similar number of stars to the globular cluster itself (i.e. of order 1,000 stars), and at much lower surface density compared to the background field population. Moreover, as argued in § 3.2.1 and also apparent in Figure 8, the averaged heating of many such encounters is negligible compared to responses to higher mass subhalos. We conclude that it is unlikely that the smaller subhalos would leave an observable signature in Pal 5’s stellar streams.

4.3. Stellar Streams in Λ CDM

To assess the integrated effect of subhalo encounters, we would ideally run simulations of streams evolving in the presence of dark-matter subhalos from the full Λ CDM spectrum. However, as outlined in §4.2, close encounters play a decisive role in shaping streams. Hence, we limit our computational expense by selecting only the 97,090 subhalos which enter within a Galactocentric radius of 25kpc at least once during the 8.44Gyr fiducial simulation time from our full realization of over 300,000 subhalos in the mass range $10^5 - 10^{10} M_\odot$.

Figure 9 summarizes the results of 12 such simulations with projections of the final particle positions, centered on the satellite body, onto the x-y plane. All the simulations were of the same stream, but started one radial orbital period apart in order to explore a variety of encounter histories. The difference between the panels is most striking. These simulations were designed so that all the streams would end with the same shape and orbital phase (although different lengths) in the absence of interactions with dark-matter subhalos. Instead, the

streams show a wide variety of morphologies and orbital phases, that can largely be attributed to the few encounters with the more massive dark-matter halos (those likely to be observed as stellar satellites).

Nevertheless, in one way the streams are *similar*: they all show tens of small-scale ($\sim 1\text{kpc}$ and below) gaps, caused by the many less-massive subhalos — the missing satellites. The frequency of these encounters means that these disturbances are apparent in all cases. In this sense, we agree with (Carlberg 2009) that any observed thin stream should contain the signatures of missing satellites. However, it is not clear from Figure 9 that the mere existence of old streams rules out the presence of a large population of low-mass dark-matter subhalos — many examples of thin, old streams survive in our simulations. Indeed, Figure 9 suggests that we might expect to find remnants of destroyed streams at surface brightness levels below the current level of sensitivity.

The gaps themselves have a striking morphology: their edges are typically not perpendicular to the stream, but rather sit at an angle. This “slant” is particularly noticeable for debris at the orbital apocenter. We can trace this appearance in coordinate space to back to the character of the gaps seen in energy/angular-momentum-space in earlier figures. The edges of the gaps typically have a single orbital energy with a range of angular-momenta. As the debris spreads, the particles sort themselves in energy along the stream and in angular momenta perpendicular to the stream (Johnston et al. 2001), which results in the angular momenta of particles varying monotonically along the edge of a gap. The slant reflects the corresponding monotonic trend in the particles’ orbital time periods, which are weakly dependent on angular-momentum.

There are also examples of bizarre morphologies in the streams in Figure 9. Several streams have discontinuities as large as several kpc (for example in the middle right-hand and bottom left-hand panel) — sufficiently disjointed that theses structure might be detected as separate streams when we observe them. (Note that the gap between the leading and trailing streams in each panel is due to the initial conditions in the simulation and not subhalo interactions.)

Some streams even take on a bifurcated appearance, for example in the third panel in the middle row and the rightmost panel in the bottom row of Figure 9. The lower panels of Figure 10 show the final energy/angular-momentum distributions for these bifurcated streams, with the redder and purpler particles having initially higher and lower energy respectively. Comparing this to the initial distribution in Figure 2 shows that in both cases, the energy-angular momentum distributions have been completely flipped by an encounter with a large subhalo, so that the trailing stream ends up on orbits with shorter time periods and overtakes the leading stream. A bifurcation has already been seen in the stellar stream from Sgr (Belokurov et al. 2006c) and could possibly be due to such an encounter. However, further simulations of an Sgr-scale stream (much longer and thicker than our Pal-5-like test case) are needed to confirm the plausibility of this scenario and distinguish it from other explanations of this bifurcation (e.g. Fellhauer et al. 2006; Peñarrubia et al. 2010). We do not pursue this investigation further here since we are concentrating on encoun-

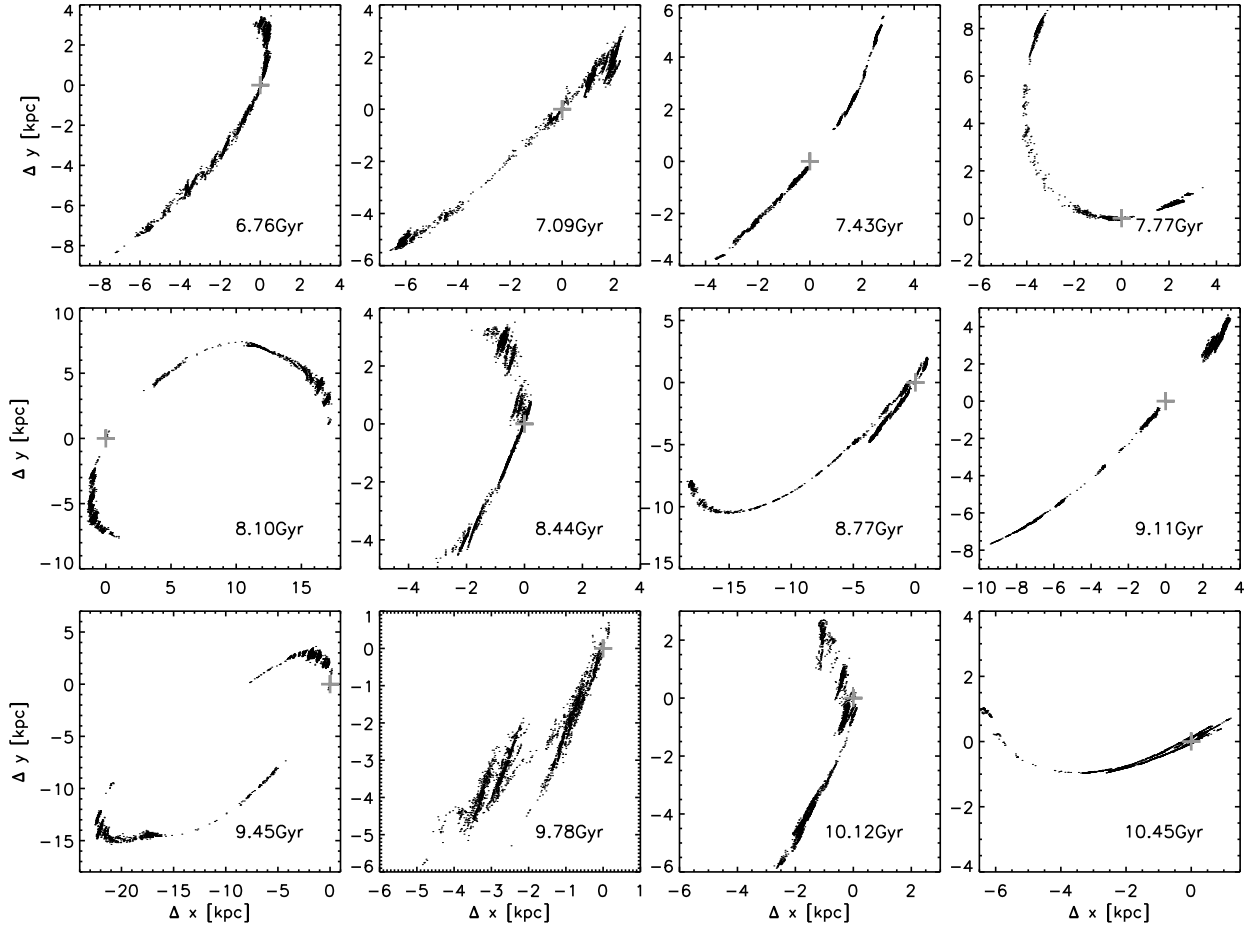


Figure 9. Final particle positions in the X-Y plane for tidal streams evolved in the presence of the full spectrum of Λ CDM subhalos. Each stream begins at differing initial times and positions that were chosen to place all streams at the same ending location in the absence of other disturbances (see the text). The age is presented in each panel. Note that each panel is centered on the satellite and has a different axis scale.

ters of missing satellites with much colder streams.

5. DISCUSSION

Our results suggest that missing satellites, if present with number densities predicted by purely dark matter simulations of structure formation in a Λ CDM Universe, should leave their imprint on cold stellar streams such as Pal 5 and GD-1 in the form of abrupt changes in surface density and velocity on few degree-scales and below. Moreover, this signature should be distinct from the few larger-scale deformities expected to be produced by known satellites. In this section, we compare our numerical results to current observations and discuss other possible explanations of substructure in stellar streams.

5.1. The Case of Pal 5: Signatures of Missing Satellites

The most straight forward thing to observe about stars in a stream with current capabilities are their positions on the sky. In reality, cold streams like Pal 5 have been discovered as *overdensities* of stars that lie along a restricted sequence in color-magnitude space (defined by a stellar isochrone), rather than direct identification of individual stellar members. The identification process requires some kind of binning or smoothing of the stars

in order to decide if a region is overdense, and this will soften any inhomogeneities in the stream. For example, Figure 3 of Odenkirchen et al. (2003); Grillmair (2009) present maps of the region around Pal 5, in which the star counts have been smoothed with a parabolic and gaussian kernel. For comparison, we select three model streams among the ones in Figure 9, count the particles in $24' \times 24'$ bins (chosen to mimic the level of smoothing in the original maps) and present contours of surface density in Figure 11. Odenkirchen et al. (2003) found 1,650 stars in a 10° length of stream, and we expect comparable surface densities for our particles (of which there are 3,000 in about 25°). Hence we choose the same contour levels as Odenkirchen et al. (2003) at the 1.5, 2, 3, 5- σ , and higher levels, with $\sigma = 0.12$ particles/arcmin². The largest gaps around RA=227°, 243°, and 231° in each panel arise from initial conditions (the physical separation of the leading and trailing streams) and not subhalo encounters. Aside from them, we still find many gaps and clumpy substructures in each stream which — while somewhat more exaggerated — are in rough agreement with the observed Pal 5 stream.

Moreover, as we discussed in § 4.3, the gaps in the

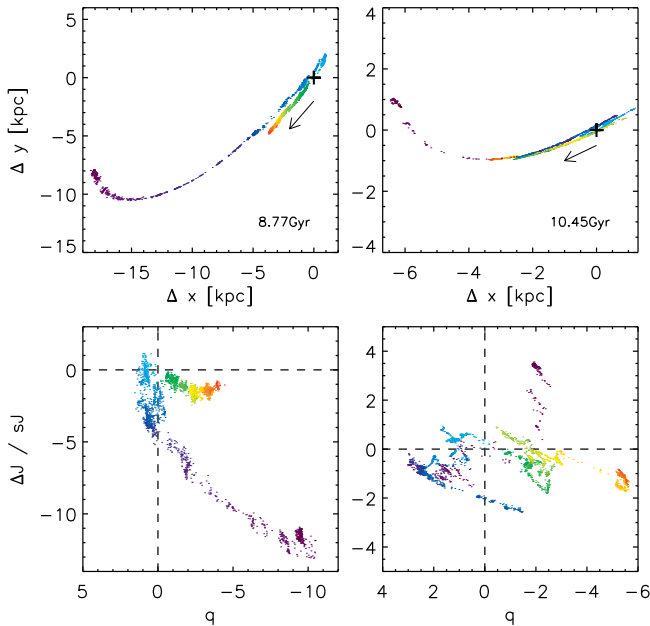


Figure 10. Two streams showing bifurcations are presented in X-Y and energy/angular-momentum planes. The arrows show the direction of the moving streams. The stream particles are color-coded by their initial energy (redder higher, purpler lower). The crossing points of dashed lines in the bottom panels show the energy and angular momentum of initial central particles (marked as crosses in the top panels).

model streams are “slanted” and this morphology is also apparent in the contour maps in the middle and right panels of Figure 11 (arrows in top and bottom panels indicated the relevant gaps). The slants are not as clear in the contour maps as in the particle plots since they are erased out by smoothing, but can become more prominent if the contour levels are varied. Indeed, in Figure 10 of Zou et al. (2009), a similar “slanted” gap is seen in the bottom-right end of the Pal 5 stream around (RA,Dec)=(227°,−2°). The distinctive gap morphology caused by subhalo encounters could provide a way of distinguishing between competing theories for the origin of stream irregularities (see next section). However, a higher density of detected stellar traces is needed to build a convincing case for the existence of slanted gaps.

While Figure 11 indicates that our simulations which included the full Λ CDM mass spectrum appear to be in rough agreement with the level of fluctuations observed in Pal 5, those that contain only the upper end (i.e. corresponding to known Milky Way satellites) are not so successful. Figure 12 shows the surface density, radial velocity dispersion, and radial velocity profiles along the streams illustrated in Figure 8, which represent simulations where the contribution of each mass decade of the full mass spectrum was isolated. The profiles are estimated from sets each containing 100 particles that have been binned in order of increasing angular separation λ from the central particle. The second and third column of panels of Figure 12 — corresponding to streams disturbed by low-mass subhalos or “missing satellites” — still reveal surface density fluctuations which are comparable to the profiles in Odenkirchen et al. (2003) and

Zou et al. (2009). However, fluctuations of the observed amplitudes and scales are *not* seen in our models that included no satellites (left hand panels), nor in those that included only the “visible” satellites from the top few decades of the Λ CDM mass spectrum (right-hand panels).

In the future, ideally we would move beyond broad consistency with the existence of missing satellites to definitively separating and measuring the contribution of each decade of the mass spectrum. This would require sensitivity to a sufficient number of stars to resolve fluctuations on sub-degree scales. A comparison of the top panels of Figure 12 with those of Figure 8 illustrates the challenge of this with our own simulated data. The difference in the nature of fluctuations caused by subhalos in the range $10^5 - 10^6 M_\odot$ compared to those caused by the mass decade above is striking in the particle plots, but the binning of 100 particles to create the profiles smoothes over $\sim 30^\circ \frac{100}{3,000} = 1^\circ$ -scales so that this signature is less apparent in the density profiles.

Additional information in the form of samples of line-of-sight velocity measurements of stars in the region of Pal 5’s stream are now being collected, with the first 17 already published by Odenkirchen et al. (2009). Figure 8 demonstrates that the missing satellites scatter stars in velocity space to produce local discontinuities of a few km/s on sub-degree scales, while Figure 12 suggests that this scattering may be apparent as a small increase in dispersion in averages over a larger region. However, finding these signatures observationally remains challenging as stream stars cannot be definitively identified and any spectroscopic sample will be contaminated by interlopers.

5.2. Other Streams

There are a number of other cold streams with small widths and angular extents (and therefore ages) that rival or even surpass Pal 5 (for example, GD1, NGC5466, Acheron, Cocytos, Lethe, and Styx streams, Grillmair & Johnson 2006; Grillmair & Dionatos 2006b; Fellhauer et al. 2007; Grillmair 2009; Koposov et al. 2010). Detailed maps of these streams’ surface densities — and of any apparent gaps in them in particular — could provide complimentary probes of the missing satellites: to first order, since these streams have similar widths and all explore the inner few-10 kpc of the Galaxy we expect to find similar numbers of and scales to the signatures of encounters with dark matter lumps.

Looking ahead, a more ambitious plan would be to use multiple streams to examine the relative numbers of dark matter lumps at different Galactocentric radii. This interpretation would require rather better than simple intuitive extrapolations from the current study for the number and scales of gaps. For example, from the estimates in Koposov et al. (2010), while both Pal 5 and GD1 debris sits at similar Galactocentric radii, GD1 orbits slightly farther out (between 18-30kpc from the Galactic Center) and should perhaps therefore encounter fewer missing satellites and contain fewer gaps. However, although GD1 has a similar width to Pal 5, it has a much longer angular extent ($\sim 70^\circ$, or $\sim 40^\circ$ as viewed from the Galactic center): naively, a longer extent suggests GD 1 is the older stream, which points in the direction

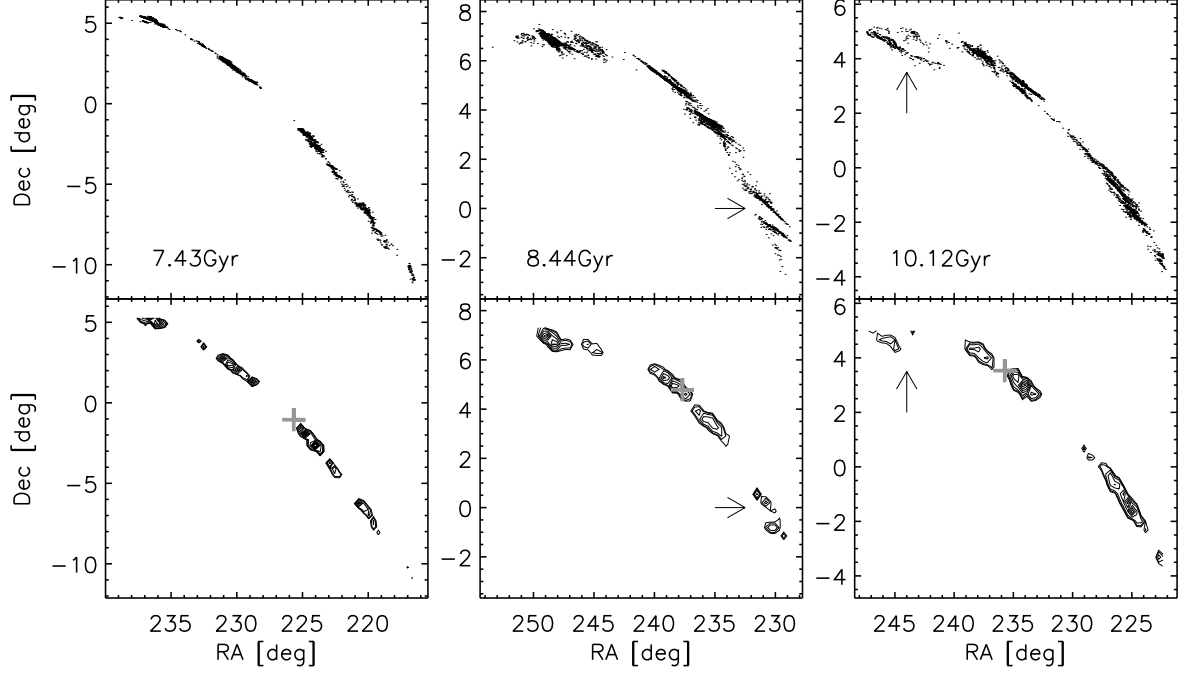


Figure 11. Particle distribution (upper panels) and surface density maps (lower panels) for three model streams from Figure 9 projected onto the plane of the sky. In the particle plots, many slanted gaps are found which are in some cases still apparent in the contour maps (indicated by arrows).

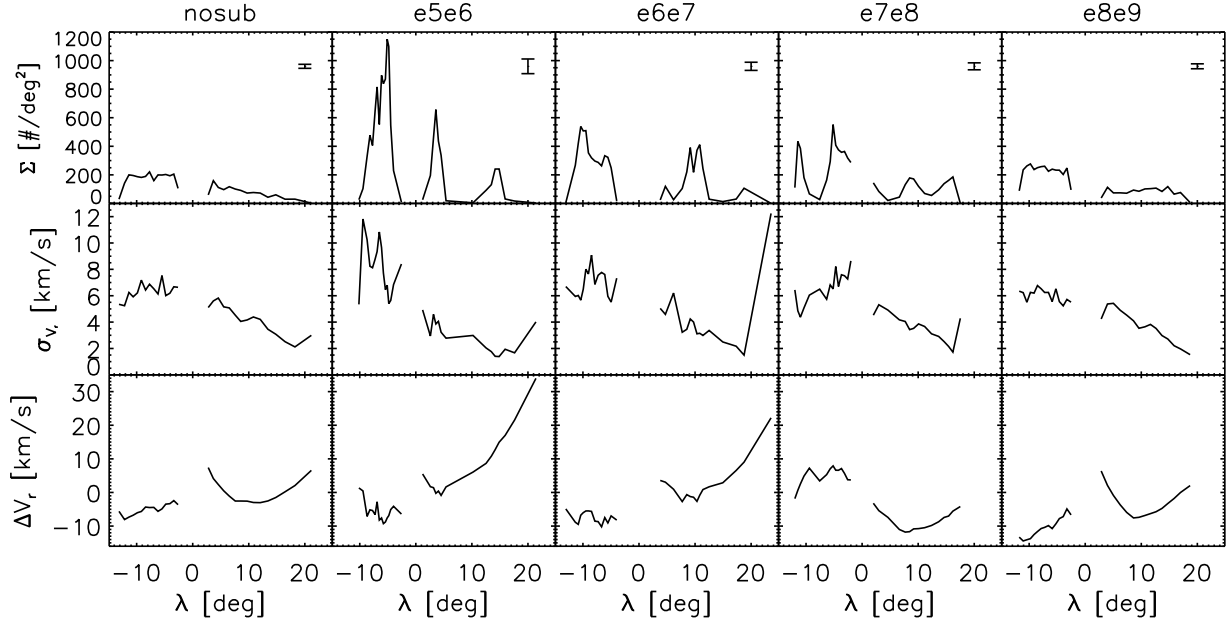


Figure 12. Top-Bottom: Number density, velocity dispersion, and radial velocity profiles along the stream. Left-Right: The stream evolved without subhalos, and with subhalos in the mass range $10^5 - 10^6 / 10^6 - 10^7 / 10^7 - 10^8 / 10^8 - 10^9 M_\odot$ are presented. λ is the angular separation from the host satellite center. Negative and positive λ mean trailing and leading stream respectively. Mean errors in the counts in the upper panels are indicated by the bar in the top-right side of the panels in the top row.

of *more* gaps. To further complicate things, GD1 is at pericenter, while Pal 5 is at apocenter, and gap scales and morphologies are phase-dependent. All these differences would have to be taken into account with specific models of each stream before any meaningful comparison could be made.

5.3. Other Influences on Stream Non-uniformity

There are several other processes that would affect the appearance of clumps in stellar streams which were not included in our numerical tests. In some cases, these could plausibly provide alternative explanations of clump origins which do not require the existence of missing satellites.

- : Multiple or continuous mass-loss events — In our simulations, the test particles all started at the same time and orbital phase, mimicking the evolution of debris from a single mass-loss event and resulting in debris in which the orbital properties of particles varied monotonically with angle along the stream. As a consequence, subhalos in our simulations directly impacted particles that were not only close physically, but also close in their orbital properties. In reality, streams are likely to be composed of stars lost over extended periods and during several mass-loss events, so that subhalos would affect debris with a wider range of orbital properties. Hence the gaps in energy space created by encounters would not be as clean as those seen in our figures (for example in Figure 8). This in turn suggests that our simulations have likely overestimated the amplitude (though not physical scales) of fluctuations in the final spatial distribution of the debris: more realistically, stars from different mass-loss populations would overtake each other across the spatial gaps and soften the contrast.
- : Asymmetries in the global potential — We assumed a purely spherical parent potential, neglecting aspherical contributions from the disk, bar, spiral arms, and Galactic warp or the (likely) triaxiality of the dark matter halo. Siegal-Gaskins & Valluri (2008) have shown in particular how the last of these can distort (relatively hot) stellar streams from large Galactic satellites. However, we anticipate that none of these large asymmetries would leave signatures that mimic the degree- and sub-degree scale gaps seen in our experiments on colder stellar streams and specifically due to direct hits by missing satellites.
- : Other sources of gravitational shocks — Streams can also suffer shocks from pericentric encounters with the Galactic bar/bulge and when passing through the Galactic disk. Disk shock, which are not taken into account in our models, can destroy globular clusters (Gnedin et al. 1999), but are not believed to be the source of discontinuities in Pal 5’s stellar streams (Dehnen et al. 2004; Küpper et al. 2010). The effect of a disk passage could be enhanced if the stream happened to pass directly through a Giant Molecular Cloud (GMC). By extrapolating the GMC mass-function, we estimate there to be of order one thousand of GMC’s within the Solar Circle

in the disk with masses $< 10^7 M_\odot$ (Solomon et al. 1987; Williams & McKee 1997), which could imply a greater density in this region than dark matter subhalos of comparable scales. However, although Pal 5 crosses the Galactic plane 35 times during the 8.44 Gyrs of our simulation, it only passes through the inner disk ($< 8\text{kpc}$) 8 times and the closest approach to the Galactic center when it crosses the disk is 7.5kpc. Hence, far less encounters of GMCs than the number of direct hits from missing satellites are expected. Overall, we conclude that the gravitational shocks from these sources should be much less frequent than encounters with subhalos for the Pal 5 stream.

- : Self gravity of the stream — Our test-particle experiments do not capture the Jean’s instability that could cause clumpy substructure in a stream even in the absence of subhalos (Quillen & Compere 2010). The importance of this effect depends on the density and velocity dispersion of the stream as well as the eccentricity of the stream orbit. Simulations including stream self-gravity are needed to assess whether it is possible to disentangle the signatures of subhalo encounters from Jeans instability.
- : Epicyclic motions of escaping stars — Küpper et al. (2008); Just et al. (2009); Küpper et al. (2010) used analytic estimates and numerical experiments to demonstrate that fluctuations in stream density can arise from epicyclic motions of escaping stars. Their experiments showed that these fluctuations should be most apparent in cases where the stars escape “evaporatively” (at low-velocity relative to the satellite) and the debris is observed at pericenter. At apocenter of their orbit with eccentricity 0.5 (comparable to Pal 5), the fluctuations appear to be less than a factor of two in amplitude and rather regularly spaced, in clear contrast to the prominent irregularly-spaced gaps induced in streams by missing satellites in our experiments.

Overall, we anticipate that the mixing of debris from multiple mass loss events could obscure the contrast and distinct morphology of the gaps seen in our idealized simulations. However, these softened fluctuations might actually be *more* consistent with those seen in observations of Pal 5’s stream. Of the remaining missing effects, the self-gravity of the stream seems to be the dominant factor confusing our interpretation and weakening our conclusion that the “missing satellites” have been found.

6. CONCLUSIONS

The goal of this study was to test if a dynamically cold stellar stream could survive in the presence of dark-matter subhalos and if so, to characterize observable features in the stream produced by subhalo encounters. In particular we were interested in finding signatures of subhalos that would be considered “missing satellites” rather than those that we already know exist. We conclude that:

1. The mere existence of cold stellar streams does not imply the absence of missing satellites — dynamically cold streams can survive for many Gyears even when bombarded by subhalos.

2. Those streams that are observed should contain the imprint of past direct impacts from subhalos in the form of gaps in surface density and discontinuities in velocities.
3. The frequency and scale of the gaps is dependent on the mass spectrum of subhalos and the properties of the stream itself. In the case of Pal 5, there should be observable fluctuations at degree and sub-degree scales due to ~ 50 encounters with subhalos in the mass range $10^5 - 10^7 M_\odot$ (i.e. the missing satellites), while distant encounters with larger subhalos produce less observable effects. Hotter stellar streams, such as Sgr's debris are large enough to hide the signatures of the many encounters it suffers with missing satellites.
4. Current observations of Pal 5's stream show that its surface density profile contains fluctuations on comparable scales to those predicted in our simulations, and could be interpreted as direct proof of the existence of missing satellites.

Our study has built on previous works to look at: effects of individual encounters with different mass scales; the distinct signatures of subhalos in different mass decades; the integrated influences of subhalo encounters; and comparisons to the current observational data. However, while we have succeeded in outlining the expected scales of signatures of different decades of the Λ CDM mass spectrum in stellar streams, there are still some open questions that need to be answered before we are confident enough to say that we have definitely found the missing satellites. In particular, self-consistent simulations of Pal 5 disruption including stream self-gravity and continuous mass loss are needed to clarify to what extent subhalo signatures could be confused by these effects. With such simulations in hand, it would then make sense to develop a multi-dimensional statistic to compare to all available data in a more robust way. The promise of current and near-future efforts to map Pal 5 and other stellar streams are strong motivators for this work.

JHY and KVJ were entirely supported by funds from Columbia University throughout this project. All simulations were run on Columbia's local computing cluster, *Hotfoot*. DWH was partially supported by the NSF (grant AST-0908357), NASA (grant NNX08AJ48G), and a research fellowship of the Alexander von Humboldt Foundation. DWH thanks Eric Bell, Jo Bovy, Andrea Maccio, and Hans-Walter Rix for useful discussions during the early stages of this project.

REFERENCES

- Belokurov, V., Evans, N. W., Irwin, M. J., Hewett, P. C., & Wilkinson, M. I. 2006a, *ApJ*, 637, L29
 Belokurov, V., et al. 2006b, *ApJ*, 647, L111
 —. 2006c, *ApJ*, 642, L137
 —. 2007, *ApJ*, 654, 897
 Binney, J. 2008, *MNRAS*, 386, L47
 Binney, J., & Tremaine, S. 2008, *Galactic Dynamics: Second Edition* (Princeton University Press)
 Bovill, M. S., & Ricotti, M. 2009, *ApJ*, 693, 1859
 Bullock, J. S. 2010, *arXiv:1009.4505*
 Bullock, J. S., Stewart, K. R., Kaplinghat, M., Tollerud, E. J., & Wolf, J. 2010, *ApJ*, 717, 1043
 Carlberg, R. G. 2009, *ApJ*, 705, L223
 Chen, J., Kravtsov, A. V., & Keeton, C. R. 2003, *ApJ*, 592, 24
 Chiba, M. 2002, *ApJ*, 565, 17
 Choi, J., Weinberg, M. D., & Katz, N. 2007, *MNRAS*, 381, 987
 Dehnen, W., Odenkirchen, M., Grebel, E. K., & Rix, H. 2004, *AJ*, 127, 2753
 Diemand, J., Kuhlen, M., & Madau, P. 2007, *ApJ*, 657, 262
 Diemand, J., Kuhlen, M., Madau, P., Zemp, M., Moore, B., Potter, D., & Stadel, J. 2008, *Nature*, 454, 735
 D'Onghia, E., Springel, V., Hernquist, L., & Keres, D. 2010, *ApJ*, 709, 1138
 Eyre, A. 2010, *MNRAS*, 403, 1999
 Fellhauer, M., Evans, N. W., Belokurov, V., Wilkinson, M. I., & Gilmore, G. 2007, *MNRAS*, 380, 749
 Fellhauer, M., et al. 2006, *ApJ*, 651, 167
 Gnedin, O. Y., Lee, H. M., & Ostriker, J. P. 1999, *ApJ*, 522, 935
 Goerdt, T., Gnedin, O. Y., Moore, B., Diemand, J., & Stadel, J. 2007, *MNRAS*, 375, 191
 Grillmair, C. J. 2006, *ApJ*, 645, L37
 —. 2009, *ApJ*, 693, 1118
 Grillmair, C. J., & Dionatos, O. 2006a, *ApJ*, 641, L37
 —. 2006b, *ApJ*, 643, L17
 Grillmair, C. J., & Johnson, R. 2006, *ApJ*, 639, L17
 Helmi, A., & White, S. D. M. 1999, *MNRAS*, 307, 495
 Hernquist, L., & Ostriker, J. P. 1992, *ApJ*, 386, 375
 Hooper, D., Kaplinghat, M., Strigari, L. E., & Zurek, K. M. 2007, *Phys. Rev. D*, 76, 103515
 Ibata, R. A., Lewis, G. F., Irwin, M. J., & Quinn, T. 2002, *MNRAS*, 332, 915
 Irwin, M. J., et al. 2007, *ApJ*, 656, L13
 Johnston, K. V. 1998, *ApJ*, 495, 297
 Johnston, K. V., Law, D. R., & Majewski, S. R. 2005, *ApJ*, 619, 800
 Johnston, K. V., Sackett, P. D., & Bullock, J. S. 2001, *ApJ*, 557, 137
 Johnston, K. V., Spergel, D. N., & Haydn, C. 2002, *ApJ*, 570, 656
 Johnston, K. V., Zhao, H., Spergel, D. N., & Hernquist, L. 1999, *ApJ*, 512, L109
 Just, A., Berczik, P., Petrov, M. I., & Ernst, A. 2009, *MNRAS*, 392, 969
 Keeton, C. R., & Moustakas, L. A. 2009, *ApJ*, 699, 1720
 Klypin, A., Kravtsov, A. V., Valenzuela, O., & Prada, F. 1999, *ApJ*, 522, 82
 Kopesov, S., et al. 2007, *ApJ*, 669, 337
 —. 2008, *ApJ*, 686, 279
 Kopesov, S. E., Rix, H., & Hogg, D. W. 2010, *ApJ*, 712, 260
 Küpper, A. H. W., Kroupa, P., Baumgardt, H., & Heggie, D. C. 2010, *MNRAS*, 401, 105
 Küpper, A. H. W., MacLeod, A., & Heggie, D. C. 2008, *MNRAS*, 387, 1248
 Lauchner, A., Powell, Jr., W. L., & Wilhelm, R. 2006, *ApJ*, 651, L33
 Law, D. R., & Majewski, S. R. 2010, *ApJ*, 714, 229
 Metcalf, R. B., Moustakas, L. A., Bunker, A. J., & Parry, I. R. 2004, *ApJ*, 607, 43
 Metcalf, R. B., & Zhao, H. 2002, *ApJ*, 567, L5
 Moore, B., Ghigna, S., Governato, F., Lake, G., Quinn, T., Stadel, J., & Tozzi, P. 1999, *ApJ*, 524, L19
 Moustakas, L. A., & Metcalf, R. B. 2003, *MNRAS*, 339, 607
 Navarro, J. F., Frenk, C. S., & White, S. D. M. 1996, *ApJ*, 462, 563
 Odenkirchen, M., Grebel, E. K., Kayser, A., Rix, H., & Dehnen, W. 2009, *AJ*, 137, 3378
 Odenkirchen, M., et al. 2001, *ApJ*, 548, L165
 —. 2003, *AJ*, 126, 2385
 Peñarrubia, J., Belokurov, V., Evans, N. W., Martínez-Delgado, D., Gilmore, G., Irwin, M., Niederste-Ostholt, M., & Zucker, D. B. 2010, *MNRAS*, 408, L26
 Quillen, A. C., & Comparetta, J. 2010, *arXiv:1002.4870*
 Quinn, D. P., Wilkinson, M. I., & Irwin, M. J. 2008, *Astronomische Nachrichten*, 329, 1071
 Riehm, T., Zackrisson, E., Mörtzell, E., & Wiik, K. 2009, *ApJ*, 700, 1552
 Siegal-Gaskins, J. M., & Valluri, M. 2008, *ApJ*, 681, 40

- Solomon, P. M., Rivolo, A. R., Barrett, J., & Yahil, A. 1987, *ApJ*, 319, 730
- Springel, V., et al. 2008, *MNRAS*, 391, 1685
- Tollerud, E. J., Bullock, J. S., Strigari, L. E., & Willman, B. 2008, *ApJ*, 688, 277
- Walsh, S. M., Jerjen, H., & Willman, B. 2007, *ApJ*, 662, L83
- Williams, J. P., & McKee, C. F. 1997, *ApJ*, 476, 166
- Willman, B., et al. 2005, *ApJ*, 626, L85
- Xu, D. D., et al. 2009, *MNRAS*, 398, 1235
- Zou, H., Wu, Z., Ma, J., & Zhou, X. 2009, *Research in Astronomy and Astrophysics*, 9, 1131
- Zucker, D. B., et al. 2006, *ApJ*, 643, L103